General Disclaimer

One or more of the Following Statements may affect this Document

- This document has been reproduced from the best copy furnished by the organizational source. It is being released in the interest of making available as much information as possible.

- This document may contain data, which exceeds the sheet parameters. It was furnished in this condition by the organizational source and is the best copy available.

- This document may contain tone-on-tone or color graphs, charts and/or pictures, which have been reproduced in black and white.

- This document is paginated as submitted by the original source.

- Portions of this document are not fully legible due to the historical nature of some of the material. However, it is the best reproduction available from the original submission.

NASA CR 167994

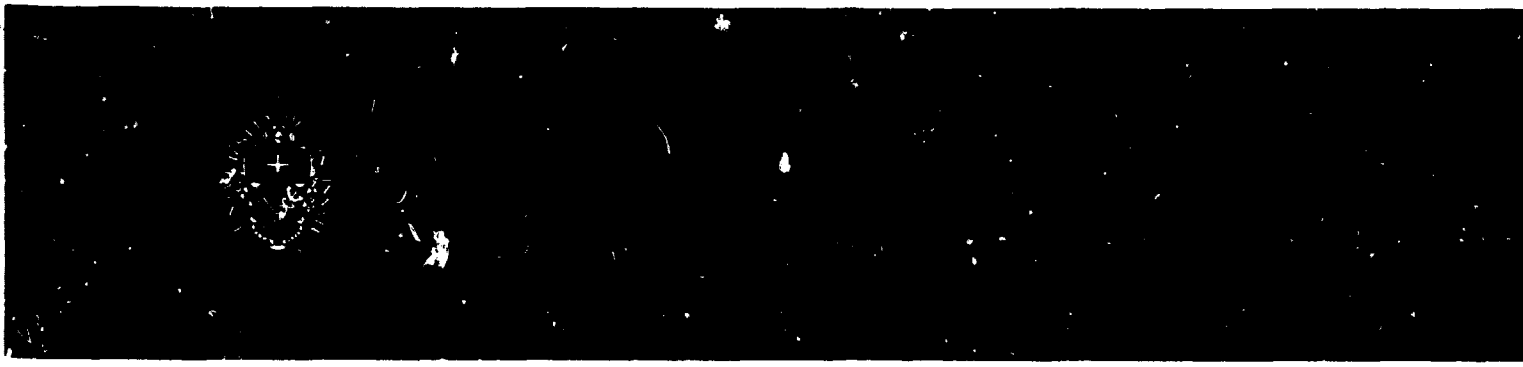

THREE-DIMENSIONAL FLOW MEASUREMENTS IN A VANELESS RADIAL TURBINE SCROLL

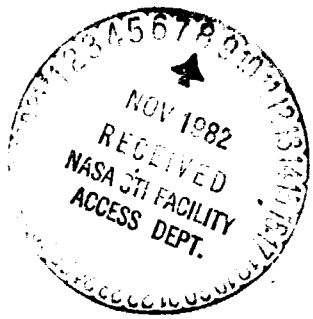

BY

W. TABAKOFF, B. WOOD AND B.V.R. VITTAL

Supported by:

NATIONAL AERONAUTICS AND SPACE ADMINISTRATION

Lewis Research Center

Grant No. NAG3-26

NASA CR 167994

THREE-DIMENSIONAL FLOW MEASUREMENTS IN A VANELESS RADIAL TURBINE SCROLL

by

W. Tabakoff, B. Wood and B.V.R. Vittal

Department of Aerospace Engineering and Applied Mechanics
University of Cincinnati
Cincinnati, Ohio 45221

Supported by:

NATIONAL AERONAUTICS AND SPACE ADMINISTRATION

Lewis Research Center

Grant No. NAG3-26

1. Report No.	2. Government Accession No.	3. Recipient's Catalog No.
CR 167994		

4. Title and Subtitle	5. Report Date
THREE-DIMENSIONAL FLOW MEASUREMENTS IN A VANELESS RADIAL TURBINE SCROLL	August 1982
	6. Performing Organization Code

7. Author(s)	8. Performing Organization Report No
W. TABAKOFF, B. WOOD and B.V.R. VITTAL	
	10. Work Unit No.

9. Performing Organization Name and Address	11. Contract or Grant No.
DEPT. OF AEROSPACE ENGINEERING & APPLIED MECHANICS UNIVERSITY OF CINCINNATI CINCINNATI, OHIO 45221	NAG3-26
	13. Type of Report and Period Covered
12. Sponsoring Agency Name and Address	Contractor Report
NATIONAL AERONAUTICS AND SPACE ADMINISTRATION LEWIS RESEARCH CENTER CLEVELAND, OHIO 44135	14. Sponsoring Agency Code

15. Supplementary Notes

Project Manager, K.L. McLallin, Turbine Aerodynamics Section, NASA Lewis Research Center, Cleveland, Ohio 44135

16. Abstract

A study was conducted to determine experimentally the flow behavior in vaneless radial turbine scroll. The data for this investigation was obtained using the slant sensor technique of hot film anemometry. This method used the unsymmetric heat transfer characteristics of a constant temperature hot film sensor to detect the flow direction and magnitude. This was achieved by obtaining a velocity vector measurement at three sensor positions with respect to the flow. The true magnitude and direction of the velocity vector was then found using these three values and a Newton-Raphson numerical technique. The through flow and secondary flow velocity components are measured at various points in three scroll sections.

17. Key Words (Suggested by Author(s))	18. Distribution Statement
Radial Turbine Aerodynamics	Unclassified - unlimited STAR Category 02

19. Security Classif. (of this report)	20. Security Classif. (of this page)	21. No. of Pages	22. Price*
UNCLASSIFIED	UNCLASSIFIED	37	

* For sale by the National Technical Information Service, Springfield, Virginia 22161

TABLE OF CONTENTS

LIST OF FIGURES

SUMMARY

A study was conducted to determine experimentally the flow behavior in a vaneless radial turbine scroll. The data for this investigation was obtained using the slant sensor technique of hot film anemometry. This method used the unsymmetric heat transfer characteristics of a constant temperature hot film sensor to detect the flow direction and magnitude. This was achieved by obtaining a velocity vector measurement at three sensor positions with respect to the flow. The true magnitude and direction of the velocity vector was then found using these three values and a Newton-Raphson numerical technique. The through flow and secondary flow velocity components are measured at various points in three scroll sections.

INTRODUCTION

The experimental investigation of flow behavior in the turbine scroll is an essential phase in the development of more efficient volute passages. Until recently very little has been known concerning flow behavior in such passages. However, one of the earliest of such investigations was conducted at the University of Cincinnati scroll research facility in 1979. In this experiment (Ref. 1) the through flow velocities of a turbine scroll, with circular passage cross-sections, were measured using a two dimensional hot wire x-probe. These results clearly demonstrated that the high speed through flow consistantly remained near the nozzle inlet. Further interpretation of the results suggested that the flow may pass through the volute with some degree of helical motion. In a latter experiment, using a three dimensional hot wire slant probe, (Ref. 2) this conjecture was confirmed. In this test both the secondary velocity vectors and the through flow velocities were measured in three passage cross-sections similar to those of the 1979 test. Although the through flow velocity data was as expected, the secondary velocity vectors formed a surprisingly interesting pattern. Two zones of secondary flow circulation were found to exist in each of the three volute cross-sections. These zones formed a split diagonally across the volute which was found to rotate clockwise with increasing distance from the inlet, thus supporting the earlier conjecture.

Most recently another set of experiments at the University of Cincinnati test facility has yielded equally interesting results. In order for the geometric influences of volute passages to be more clearly understood a turbine volute of another geometry was chosen, in this case from the Cummins Engine Company.

RESEARCH SCROLL FACILITY

The test facility was designed to incorporate a complete radial inflow turbine scroll for testing using cold air. The most recent phase of experimental investigation was concerned with the measurement of the through flow and secondary flow velocities at different scroll cross sections. It is hoped that with this data a better understanding of the scroll flow behavior will be obtained. The scroll used was vaneless with rectangular cross sections and rounded corners. The turbine rotor was modified in such a way that the blades were removed and only the rotor hub was used in its place.

Figure 1 shows the schematic diagram of experimental set-up. High pressure air was supplied from four large storage tanks. The air passed through a remotely controlled pressure regulating valve, standard orifice meter, filter and a flow regulating valve before entering the settling chamber. The temperature of the air was measured in the settling chamber. The filter was used to trap dust particles up to a nominal diameter of about three microns. This prolonged the operating life of the hot film sensor.

The air supply was regulated by the flow regulating valve to give an air mass flow of 0.181 kg/sec (0.4 lb/sec). The air mass flow was measured by a standard orifice meter. The air from the settling chamber was fed to the scroll inlet through a convergent duct. The duct was circular in shape and blended smoothly into the inlet of the scroll.

EXPERIMENTAL APPARATUS

The volute geometry was such that a slot cut in the upper volute wall allowed the probe to access any point within a passage. The slot was then covered with a moveable plate mounted on teflon bearings. The plate was fabricated with a special port which allowed the probe and its associated traversing apparatus to be attached. This entire assembly allowed the probe to reach any desired point within a passage while (Figs. 2 and 3) at the same time providing an air tight seal. The slot and air seal construction was such that the volute flow was not disturbed. This was achieved by minimizing the slot dimensions and eliminating any unnecessary protrusions into the flow path.

Three widely spaced cross sections were chosen for the tests. The first position was located just downstream of the tongue location and the subsequent two positions were at 90 degree intervals (Fig. 4). This permitted the possible variations in scroll flow due to geometric effects to be evident. The turbine blades were also removed and replaced with a smooth center-body which was modeled from the turbine hub. This allowed flow variations due only to volute passage geometry to be studied.

Scroll Geometry:

Since curvilinear flow channels with variable cross-sections offer no characteristic length, Reynolds number ($\bar{V}d/\nu$) alone based on the average velocity $\bar{V}$ of steady flow ceases to be a criterion of describing the flow, as it is used for straight pipe flow. However, a simple dimensional analysis carried out suggests that such flow can be geometrically and dynamically

compared by defining two nondimensional numbers, namely: $(\rho Q/\mu d)$ and R/d where Q is the volume flow rate. The former is nothing but a modified Reynolds number. In this work the scroll inlet mass flow Reynolds number was defined as $(\rho V_{ave} d_h/\mu)$ and was equal to 2.044×10^5 and the parameter R/d_h was equal to 2.3. Figure 4 shows three scroll section locations. The first cross section is at $\phi = 0°$, the second at $\phi = 90°$ and the third at $\phi = 180°$.

Instrumentation:

The air mass flow was measured using a standard orifice meter. The temperature of the air was measured in the settling chamber using a simple commercial dial type thermometer with a stem. No pressure measurements were made except at the orifice meter. The velocity measurements inside the scroll were made using the TSI model 1213-20 hot film slant sensor. The schematic diagram of the sensor is shown in Fig. 5. The cylindrical sensor element is 0.0508 mm (0.002 in.) in diameter, 1.016 mm (0.040 in.) long, and is at a slant angle of 45°. It is coated with alumina and gold plated at the ends where it is fixed to the prongs. The prongs are 12.7 mm (0.5 in.) long.

Probe Mount and Flow Measurement:

The positions of three scroll cross sections where the measurements have been taken are shown in Fig. 4. At each section, a specially designed probe traversing fixture to suit the section geometry, was used. Narrow slots were cut in the upper cross sectional walls, which allowed the probe to access any point within a particular cross section. Flat sliding plates, to which the traversing mechanism was attached, were

mounted on bearings over the slots. This system allowed the probe to be positioned at any depth, using the traversing mechanism, and at any distance from the side walls, using the sliding plates.

Procedure:

The high pressure air supply from air storage tanks was regulated to a pressure of 2.0684×10^5 N/m^2 gauge (30 psig) at the orifice meter using a pressure regulating valve. The air supply was passed through an air filter to a settling chamber where the temperature was measured. The pressure drop across the orifice meter was varied with the flow regulating valve to give an actual air mass flow of 0.181 kg/sec (0.4 lb/sec). The air temperature did not vary appreciably from the nominal temperature of 22°C (72°F).

The flow velocity measurements inside the scroll were made using a hot film slant sensor. It was advantageous to use this sensor for three dimensional flow measurements since it required only one channel of electronic circuitry, when compared to two or three for cross wire probes. This consequently minimized measurement errors. Also, the obstruction to the flow field was reduced. The operation, calibration and the evaluation of velocities from the anemometer output signals are explained in Appendix A.

TABLE 1

THE SCROLL INLET VELOCITY DISTRIBUTION

Angular Position θ (deg) (Fig. 6)	Depth (cm)	Through Flow Velocity V_x (m/sec)
0	0.635	46.3
	1.27	47.5
	1.905	47.5
	2.54	48.4
	3.175	49.3
	3.81	49.6
	4.445	49.2
	5.08	50.2
	5.715	50.4
90	1.27	46.4
	1.905	46.6
	2.54	49.2
	3.81	51.0
	4.445	50.6

RESULTS AND DISCUSSION

The scroll inlet velocity measurements were made at two port locations. The results are shown in Fig. 6 and Table 1. The inlet velocities did not vary much (within ±5%). The velocities tend to be higher near the outside wall of the scroll. The total velocity vector at every point of measurement in the scroll cross sections was resolved into three components. The through flow component, V_x, and the two secondary flow components V_h and V_v. Figures 7, 8 and 9 show the measured through flow velocities in each of the three sections. For all the measurements, the mass flow rate was maintained at 0.1811 kg/sec (0.4 lb/sec). The numerical values of the flow velocity components at various locations in the scroll are given in Appendix B.

The secondary flow vectors have been presented graphically in two forms. The resultant velocity vectors and their horizontal components have been superimposed on twice scale drawings of each test section. All of the velocity vectors have been presented at a scale of 1. cm = 12 m/sec. For the cases which have complicated secondary flow paths, estimations of the flow paths have been drawn. The through flow velocity contours have been plot ed in cross-sectional drawings of twice scale. In all cross-sectional drawings the through flow velocity vectors pointed into the cross-sectional plane.

The data obtained from the first test cross-section demonstrated the flow's immediate response to the nozzle discharge. Although the first series of tests were conducted only 1 cm downstream from the tongue location, the high speed flow had already adjusted its position. The secondary flow resultant

vectors (Fig. 10) and their horizontal components (Fig. 11) showed a uniform secondary motion toward the outer volute wall. It should be noticed, however, that the fluid at this point had not yet passed through the curved portion of the volute passage.

The second test cross-section, however, was located 90 degrees from the first. The fluid had, therefore, adjusted both to the nozzle's discharge and the 90 degree passage bend. The through flow velocity contour (Fig. 8) shows little change from the pattern of the first test section, although a substantial increase in velocity has occurred. However, the secondary vectors show a dramatic change. The resultant vectors (Fig. 12) show that two zones of secondary circulation have formed in response to the forces imposed on the fluid at this point. The vertical split which separated the circulation zones can clearly be seen from the secondary flow horizontal components (Fig. 13). The zones appear to have rotated in a counter clockwise direction near the outer volute wall and in a clockwise direction near the inner wall. The estimated path of these circulation zones is shown in Fig. 14. The formation of the zones of circulation is undoubtedly due to the nozzle discharge as well as the centrifugal forces imposed by the passage turning angle.

The test readings obtained 180 degrees from the first test cross section indicated that the turbulence level had greatly increased. The flow characteristics, however, were similar in nature to those of the second section tested. As illustrated by

the secondary flow resultant vectors and their horizontal components (Figs. 15 and 16), a reasonably stable flow pattern seems to have formed. The split location and the secondary flow path (Fig. 17) were virtually identical to those of the second cross section tested. The same clockwise and counter-clockwise secondary motion existed near the volute's inside and outside walls respectively. However, there appears to have been a shift in the location of maximum secondary velocity. This was no doubt due to the nozzle's more vertically symmetric position on the inside wall. The through flow velocities were again highest near the scroll inner wall (Fig. 9), although the maximum velocities were somewhat less than those of the second test section. The through flow profiles were also much less uniform immediately before the nozzle in this case. This may also be attributed to the variation of nozzle position.

CONCLUSIONS

This series of tests has again demonstrated the great influence which volute geometry has on flow behavior. Several of the conjectures proposed in the earlier turbine volute research projects have been reinforced by this latest work. For example, both the first and second experiments conducted at the University of Cincinnati's test facility strongly suggested that a helical motion was present in flow through turbine volutes of circular cross-sections. This test series, since the scroll cross-section geometry was nearly rectangular,

has by contrast demonstrated that this motion was apparently induced by the passage's cross-sectional shape. For example, there was no evident rotational motion of the secondary flow split location between the 90 degree and the 180 degree test cross-sections of this latest series of tests. Contrary to this, the earlier tests at the University of Cincinnati have shown significant rotational motion of the secondary flow split location.

The absence of a secondary flow split in the first test cross-section and its dramatic appearance at the 90 degree location, of this latest work, also tends to confirm earlier speculation that the secondary flow split was formed in reaction to both the forces imposed by the nozzle and the centrifugal forces imposed by the passage bend.

Smaller variations in the secondary flow patterns of the latest volute tests appear to have been largely due to variations of the nozzle position on the volute wall. For example, directly in front of the nozzle the secondary flow velocities were typically higher than at other locations within a test cross-section. Due to the construction of this volute, the nozzle position increased in altitude along the inside volute wall with increasing depth into the scroll. This of course affected the location of maximum secondary flow and to some extent the pattern of secondary flow.

ACKNOWLEDGEMENT

The University of Cincinnati and the authors wish to thank the administrators and the technical personnel of the Cummins Engine Company, Columbus, Indiana, for the donation of the scroll geometry and their useful discussions in regard to this research work.

REFERENCES

1. Tabakoff, W., Sheoran, Y., Kroll, K., "Flow Measurements in a Turbine Scroll," ASME Journal of Fluids Engineering, September 1980, Vol. 102.
2. Tabakoff, W., Vittal, B.V.R. and Wood, B., "Three Dimensional Flow Measurements in a Turbine Scroll," NASA CR-167920 Report, 1982.
3. Schmidt, D.P. and Okiishi, T.H., "Multistage Axial-Flow Turbomachine Wake Production, Transport, and Interaction," Engineering Research Institute, Iowa State University, Ames, Iowa 50010.

NOMENCLATURE

b	empirical calibration coefficients
d	diameter of the scroll cross section, m
d_h	hydraulic diameter of the scroll section, m
M	sensor rotation angles, deg.
Q	volume flow rate, m^3/sec
R	radius of curvature of the scroll, m
$\bar{V}$	flow velocity vector, m/sec
V_{ave}	average velocity, m/sec
V_e	effective cooling velocity, m/sec
V_h	horizontal component of the secondary flow velocity, m/sec
V_s	secondary flow velocity, m/sec
V_v	vertical component of the secondary flow velocity, m/sec
V_x	through flow component of velocity, m/sec
α	sensor yaw angle, deg. (Fig. 5)
θ_0	slant angle, deg. (Fig. 5)
θ_p	probe pitch angle, deg. (Fig. 5)
θ_y	probe yaw angle, deg. (Fig. 5)
μ	dynamic viscosity, kg/m sec
ν	kinematic viscosity, m^2/sec
ρ	density, kg/m^3
ϕ	scroll angular coordinate, deg.

APPENDIX A

MEASUREMENT TECHNIQUES

The same slant hot film techniques (Ref. 3) was used as in the preceding volute test (Ref. 2). This method used three probe voltage readings, taken at three angular positions, to produce a single velocity vector measurement. This was accomplished through the use of a set of second order empirical correlations.

The method maintained a thin sensor wire, covered with a conductive coating, at a constant temperature by passing an electrical current through the coating. Since the wire temperature was higher than that of the scroll air flow, the air passing over the sensor had a cooling effect. The probe's directional measurement ability was due to these heat transfer qualities. The sensor slant angle and nonuniformities in the conductive coating created non-symmetric heat transfer traits with regard to the air flow direction. The changes in heat transfer were of course represented by corresponding changes in the voltage, needed to maintain the sensor wire at a constant temperature. This allowed the writing of a second order empirical relation between the probe voltage and the air flow velocity vector.

$$V_e/V = b_0 + b_1 \alpha + b_2 \theta_p + b_3 V + b_4 \alpha^2 + b_5 \theta_p^2 + b_6 V^2 + b_7 \alpha\theta_p + b_8 \alpha V + b_9 \theta_p V \quad (1)$$

The 'b' coefficients were obtained during the calibration process and were unique to every probe. They, infact, represented the probe's voltage response to all flow situations. Their values were determined by using equation (1) in a least squares curve fit between a known and precisely controlled calibration air stream vector, air speed and direction, and the probes voltage response to the flow situation. This necessitated the acquisition of voltage responses to the air speed magnitudes and directions which were expected during the scroll tests. The probe was, therefore, placed in a calibration air flow and swept through the yaw and pitch angles which were expected to be encountered during testing. A set of angular sweeps was conducted for each calibration air speed. The air speeds were, in general, chosen at 15ft/second intervals over the entire range of air speeds expected during actual testing.

The α, in this case, was an angle which geometrically related the sensor's pitch angle, yaw angle, and slant angle. The relationship developed to express this was given by the following equation

$$\cos \alpha = \cos \theta_0 \cos \theta_p \cos \theta_y + \sin \theta_0 \sin \theta_p \qquad (2)$$

where θ_p was the sensor pitch angle relative to the flow direction, θ_y was the sensor yaw angle relative to the flow direction, and θ_0 the sensor slant angle (Fig. 5).

The unknowns of equations (1) and (2) were, of course, the pitch angle, yaw angle, α, and the velocity. The value of V_e the effective cooling velocity, was directly related to the probe voltage and was, therefore, known for each velocity measurement

made. In order to solve for these unknowns a scheme was developed (Ref. 3) to make this a determinate system of equations. It was found that this was best accomplished by making three measurements for each velocity vector. This created a system of six equations and six unknowns for each velocity vector measured. This system of equations was given by:

(a) $$V_{e_a}/V = b_0 + b_1 \alpha_a + b_2 \theta_p + b_3 V + b_4 \alpha_a^2 + b_5 \theta_p^2 + b_6 V^2 + b_7 \alpha_a \theta_p + b_8 \alpha_a V + b_9 \theta_p V$$

$$\cos \alpha_a = \cos \theta_0 \cos \theta_p \cos \theta_y + \sin \theta_0 \sin \theta_p$$

(b) $$V_{e_b}/V = b_0 + b_1 \alpha_b + b_2 \theta_p + b_3 V + b_4 \alpha_b^2 + b_5 \theta_p^2 + b_6 V^2 + b_7 \alpha_b \theta_p + b_8 \alpha_b V + b_9 \theta_p V$$

$$\cos \alpha_b = \cos \theta_0 \cos \theta_p \cos(\theta_y - M_b) + \sin \theta_0 \sin \theta_p$$

(c) $$V_{e_c}/V = b_0 + b_1 \alpha_c + b_2 \theta_p + b_3 V + b_4 \alpha_b^2 + b_5 \theta_p^2 + b_6 V^2 + b_7 \alpha_b \theta_p + b_8 \alpha_b V + b_9 \theta_p V$$

$$\cos \alpha_c = \cos \theta_0 \cos \theta_p \cos(\theta_y - M_c) + \sin \theta_0 \sin \theta_p$$

The six unknowns were then α_a, α_b, α_c, θ_p, θ_y, and V. Each equation set (a,b,c) represented the measurement of the velocity vector at one of three yaw angle positions which were given by the relations

θ_y, $\theta_y - M_b$, and $\theta_y - M_c$ (Fig. 18). Although the exact yaw angle was not known until completion of the data reduction process, the first probe V_e reading was taken with the sensor turned to a five degree yaw angle position with respect to the air flow. Therefore, the first V_e reading was taken at a yaw angle, θ_{y_a}, of five degrees. This was accomplished through the observation of probe voltage characteristics. V_e readings were then taken at a positive angular position $\theta_{y_b} = \theta_{y_a} + M_b$ and at a negative angular position $\theta_{y_c} = \theta_{y_a} - M_c$. In this experiment M_b and M_c were chosen to be 30 degrees in the clockwise and counter-clockwise directions respectively. The corresponding effective cooling velocities were then used in the above system of empirical relations to determine the six unknown quantities. This, of course, was sufficient to produce the velocity vector's direction and magnitude relative to the sensor wire. A Newton-Raphson numerical technique was developed to solve this sytem of equations providing that an estimation of pitch angle, yaw angle, and total velocity was given. It was found that a very rough estimate was sufficient to assure convergence of the scheme. A set of trigonometric relations was then used to transfer the velocity vectors from the coordinate system relative to the sensor wire to the secondary and through flow scroll air flow velocity components.

APPENDIX B

SCROLL SECTION I

Distance From Inner Wall (cm)	Depth From Reference Point * (cm)	Through Flow Velocity (m/sec) V_x	Secondary Flow Velocity (m/sec)		
			Vertical Component V_v	Horizontal Component V_h	Resultant V_s
1.5875	0.3175	54.67	6.86	- 2.10	7.18
1.5875	0.6350	57.02	6.69	0.12	6.69
1.5875	1.2700	61.25	8.71	- 6.95	11.14
1.5875	1.9050	61.95	7.59	- 5.63	9.44
1.5875	3.1750	63.49	6.64	-14.20	15.68
1.5875	3.8100	64.57	5.21	-13.93	14.87
1.5875	4.4450	66.34	5.13	-14.51	15.39
1.5875	4.7625	67.68	4.96	-13.95	14.80
2.2225	0.0	50.90	1.77	- 1.92	2.62
2.2225	1.2700	59.46	7.63	- 6.83	10.24
2.2225	1.9050	60.44	6.39	- 5.53	8.45
2.2225	2.5400	60.54	7.75	-14.23	16.21
2.2225	3.1750	61.58	7.62	-14.48	16.37
2.2225	3.8100	62.56	7.03	-14.96	16.53
2.2225	4.4450	62.97	5.28	-14.21	15.16
2.2225	5.0800	65.12	6.29	-15.20	16.45
2.8575	0.0	49.21	1.61	- 9.84	9.98
2.8575	0.6350	53.97	6.21	- 8.64	10.64
2.8575	1.2700	55.75	6.87	- 7.90	10.47
2.8575	1.9050	56.96	6.97	- 6.96	9.85
2.8575	2.5400	57.41	6.29	- 6.34	8.93
2.8575	3.1750	58.74	6.64	- 5.37	8.54
2.8575	3.8100	58.72	5.04	- 4.66	6.86
2.8575	4.4450	60.55	5.04	- 4.62	6.84
3.4925	0.6350	51.94	5.31	- 9.01	10.46
3.4925	1.2700	54.33	6.57	- 8.47	10.72
3.4925	1.9050	54.10	5.49	- 7.46	9.26
3.4925	2.5400	55.30	6.40	- 6.64	9.23
3.4925	3.1750	55.79	5.44	- 5.68	7.86
3.4925	3.8100	57.89	6.47	- 5.84	8.72
3.4925	4.4450	58.30	6.15	- 5.53	8.27
3.4925	5.0800	58.92	5.21	- 5.42	7.51
4.1275	0.6350	51.19	4.30	- 4.50	6.23
4.1275	1.2700	49.74	2.42	0.08	2.42
4.1275	1.9050	50.68	2.72	1.49	3.11
4.1275	2.5400	53.25	5.75	- 6.81	8.92
4.1275	3.1750	53.42	4.99	- 6.44	8.14
4.1275	3.8100	54.51	5.60	- 5.55	7.88
4.1275	4.4450	56.57	6.67	- 5.71	8.78
4.1275	4.7625	56.55	5.87	- 5.55	8.08

SCROLL SECTION 2

Distance From Inner Wall (cm)	Depth From Reference Point * (cm)	Through Flow Velocity (m/sec) V_x	Secondary Flow Velocity (m/sec)		
			Vertical Component V_v	Horizontal Component V_h	Resultant V_s
0.8890	1.2700	75.06	10.73	5.03	11.84
0.8890	2.5400	78.3	8.30	2.04	8.54
0.8890	2.1750	80.56	8.68	-11.40	14.33
0.8890	3.8100	82.33	7.46	-14.49	16.29
0.8890	4.4450	82.25	3.90	- 2.24	4.50
1.2065	1.2700	73.43	8.92	8.02	12.00
1.2065	1.9050	75.87	9.87	- 0.40	9.88
1.2065	2.5400	77.16	8.61	1.61	8.76
1.2065	3.1750	78.71	9.62	-11.90	15.30
1.9050	0.6350	68.77	5.82	4.91	7.61
1.9050	1.2700	72.43	7.21	4.82	8.67
1.9050	1.9050	71.66	7.07	- 2.12	7.38
1.9050	2.5400	72.05	5.53	0.95	5.62
1.9050	3.1750	74.03	5.00	0.30	5.00
1.9050	3.8100	74.38	5.50	0.52	5.52
1.9050	4.4450	75.51	5.94	- 0.35	5.95
1.9050	4.6990	75.00	5.03	- 0.15	5.03
2.5400	0.6350	63.51	3.31	3.82	5.05
2.5400	1.2700	64.80	3.09	7.02	7.67
2.5400	1.9050	68.02	6.77	- 2.85	7.35
2.5400	2.5400	67.01	4.54	- 0.10	4.54
2.5400	3.1750	68.41	5.64	0.32	5.64
2.5400	3.8100	69.12	5.81	- 0.09	5.81
2.5400	4.4450	70.35	6.57	- 0.27	6.57
2.5400	4.6990	70.07	5.66	- 1.13	5.77
3.1750	1.2700	59.49	3.11	- 4.89	5.79
3.1750	1.9050	61.54	4.05	2.05	4.54
3.1750	2.5400	60.98	2.78	0.51	2.83
3.1750	3.1750	62.18	4.32	1.48	4.56
3.1750	3.8100	62.41	3.38	1.70	3.78

SCROLL SECTION 3

Distance From Inner Wall (cm)	Depth From Reference Point * (cm)	Through Flow Velocity (m/sec) V_x	Secondary Flow Velocity (m/sec)		
			Vertical Component V_v	Horizontal Component V_h	Resultant V_s
0.6350	1.2700	75.50	8.03	- 5.85	9.93
0.6350	1.9050	77.96	5.32	-11.65	12.81
0.6350	2.2225	77.63	2.73	-10.91	11.25
0.6350	2.5400	78.07	1.95	-12.82	12.97
0.6350	2.8575	78.75	-0.83	- 3.65	3.74
1.2700	0.6350	71.90	6.71	2.86	7.29
1.2700	1.5875	71.83	3.63	- 3.70	5.18
1.2700	1.9050	72.35	2.35	- 0.62	2.43
1.2700	2.2225	72.97	3.24	-11.63	12.08
1.2700	2.5400	74.36	4.64	-12.38	13.22
1.2700	2.8575	72.96	0.55	- 1.84	1.92
1.2700	3.1750	74.87	2.61	- 4.17	4.92
1.2700	3.4925	77.89	6.42	- 6.95	9.46
1.9050	0.6350	66.98	4.38	2.41	5.00
1.9050	1.2700	65.39	1.47	5.61	5.80
1.9050	1.5875	67.74	5.15	- 4.24	6.67
1.9050	1.9050	67.06	2.48	- 2.49	3.52
1.9050	2.2225	67.48	1.84	- 0.99	2.09
1.9050	2.8575	70.08	2.40	- 3.05	3.88
1.9050	3.1750	71.36	3.58	- 5.03	6.17
1.9050	3.4290	71.43	4.09	- 5.43	6.79
2.5400	0.6350	63.80	4.22	- 2.88	5.11
2.5400	1.2700	59.33	-0.95	2.76	2.92
2.5400	1.5875	61.44	1.62	5.06	5.31
2.5400	2.2225	61.90	0.22	6.71	6.71
2.5400	2.5400	60.09	-3.11	6.86	7.53
2.5400	2.8575	62.29	-0.94	7.13	7.19
2.5400	3.1750	62.29	-0.94	7.13	7.19

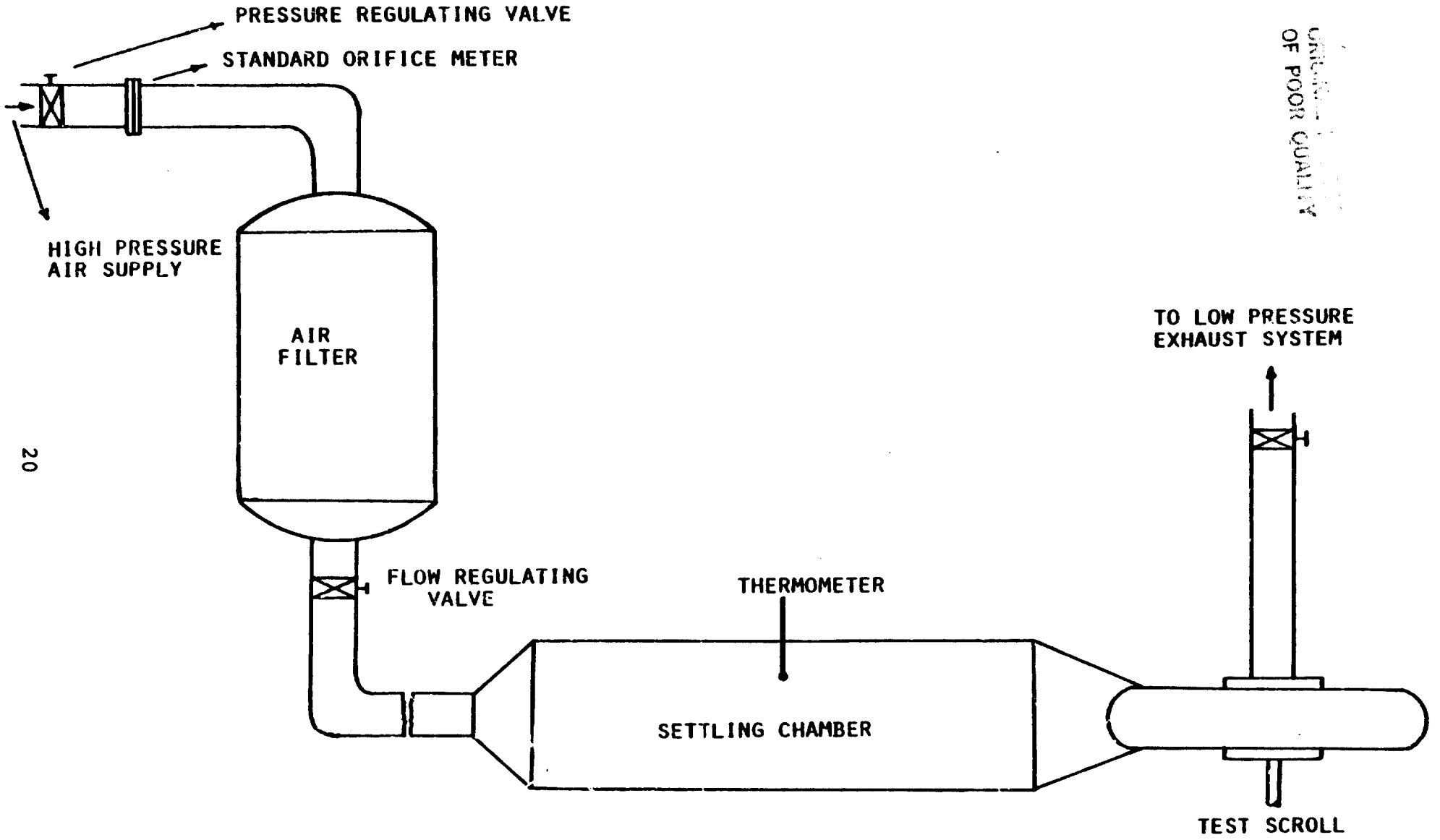

FIG. 1 . SCHEMATIC DIAGRAM OF THE EXPERIMENTAL SET-UP.

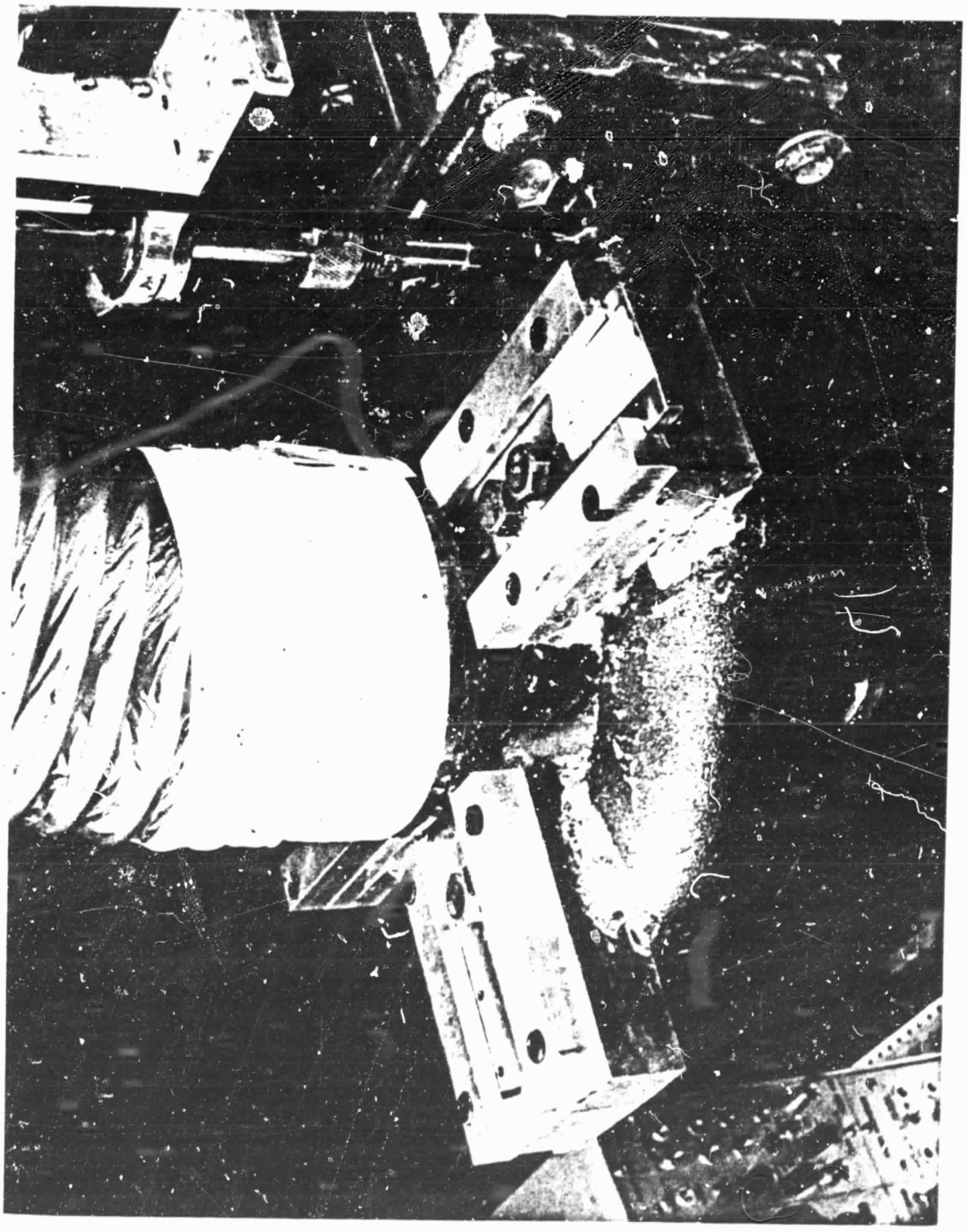

FIG. 2. SCROLL ASSEMBLY WITH THE PORT PLATES FOR THE PROBE.

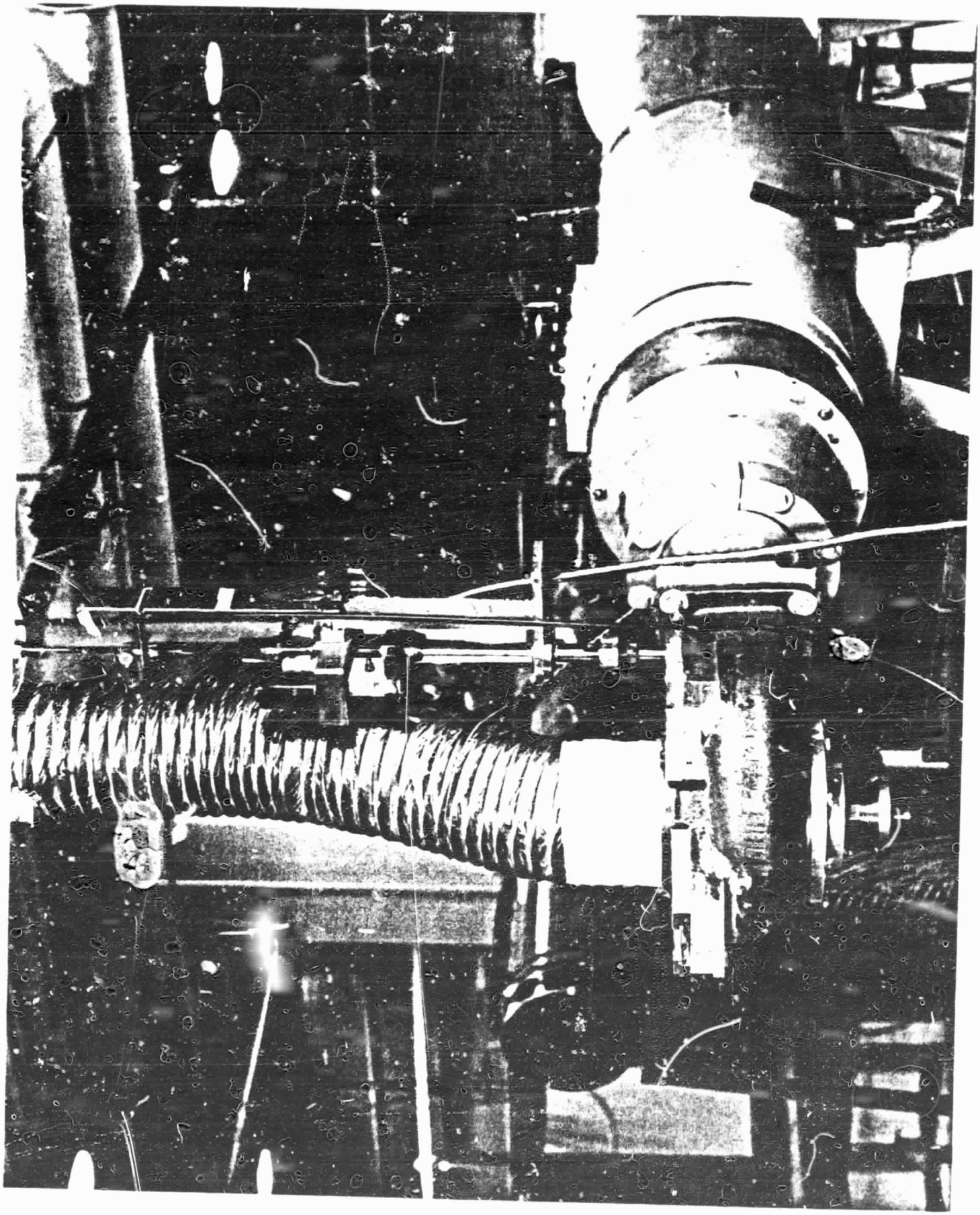

FIG. 3. SCROLL ASSEMBLY.

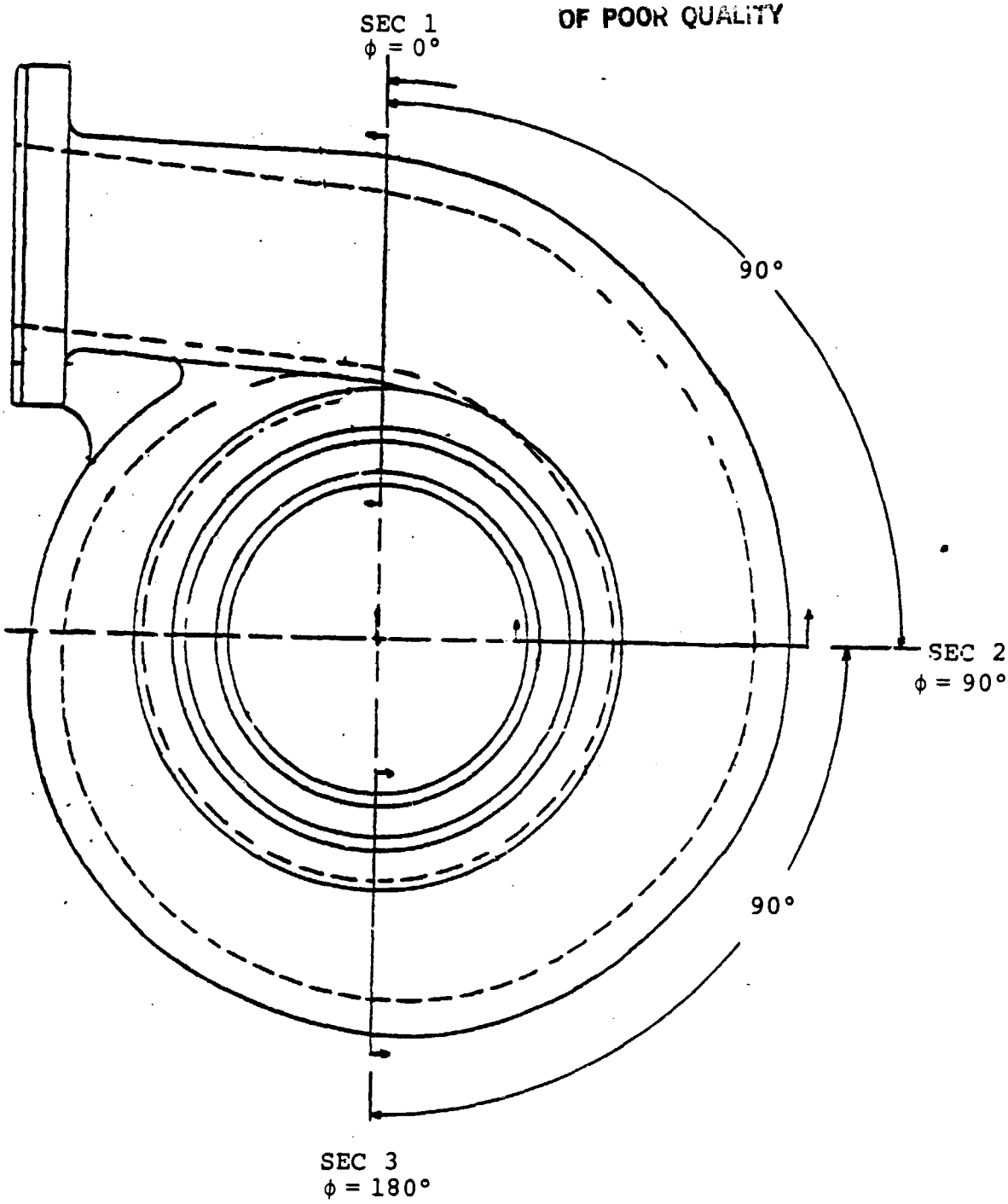

FIG. 4. SCROLL PLATFORM

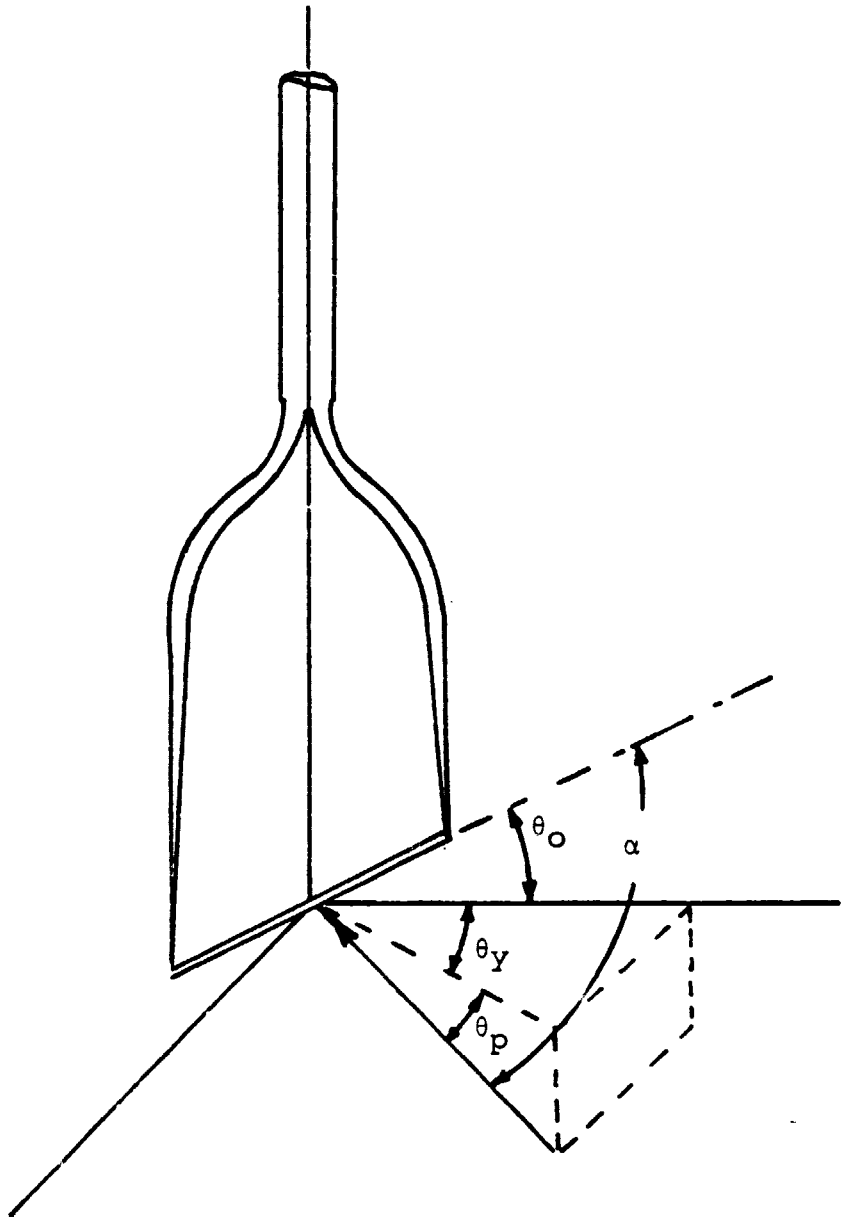

FIG. 5. PROBE GEOMETRY.

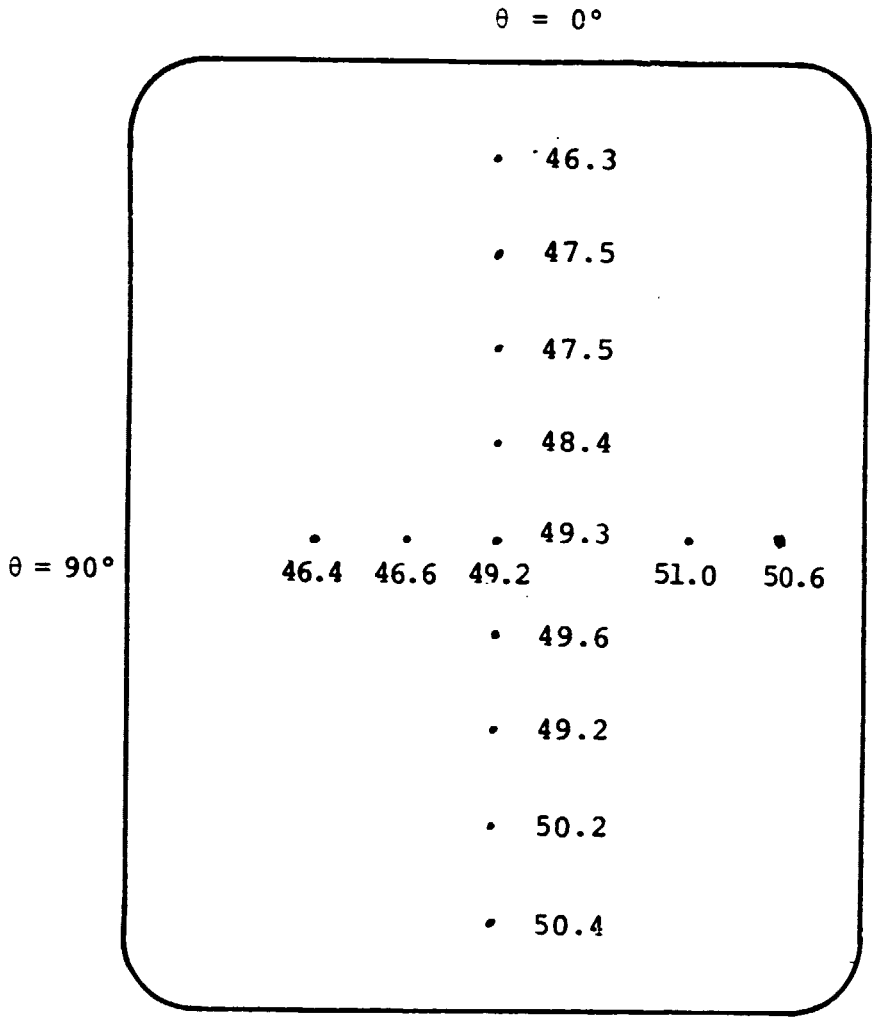

FIG. 6. INLET VELOCITY PROFILE, M/SEC.

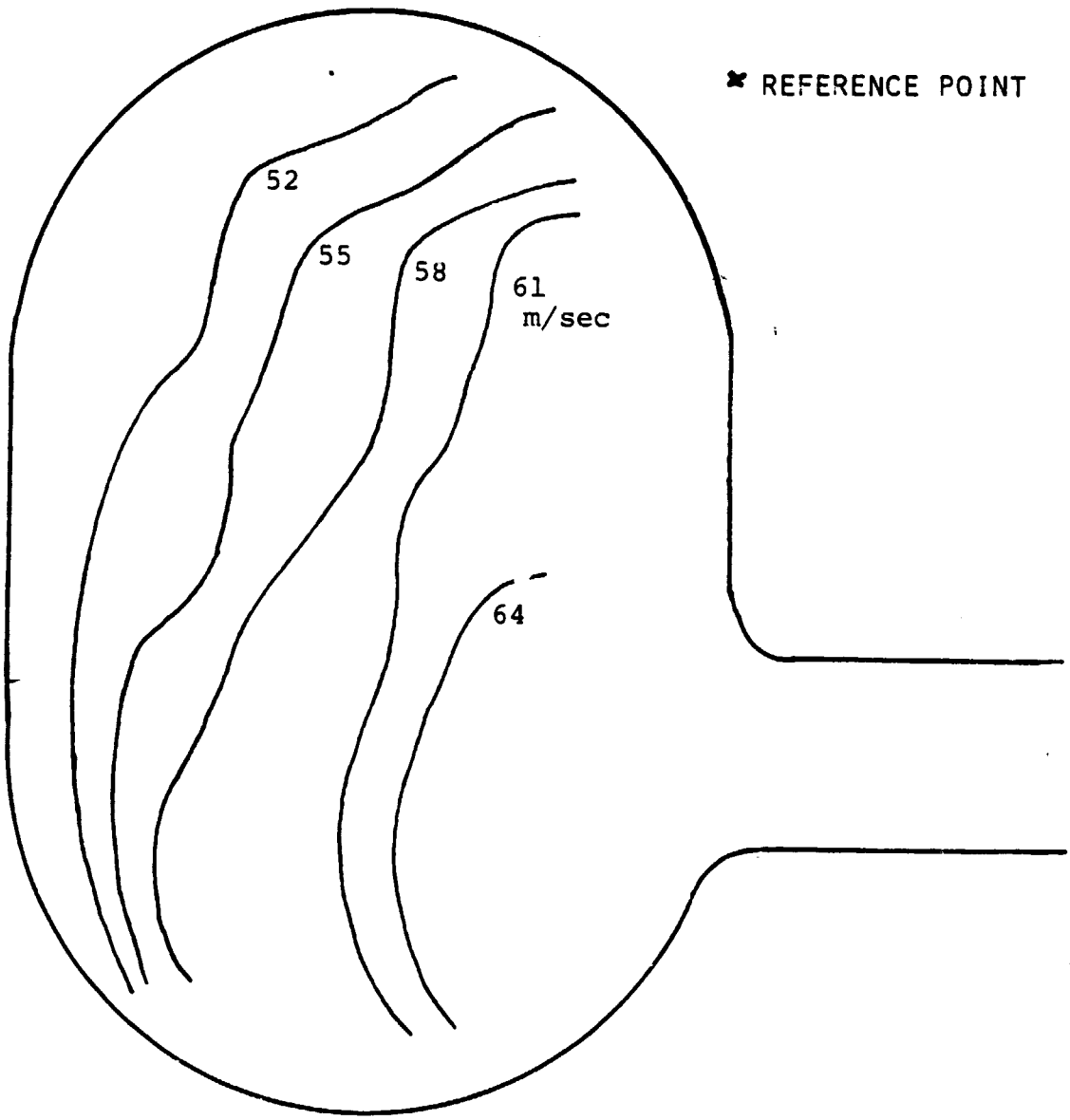

FIG. 7. THROUGH FLOW VELOCITIES, CROSS SECTION 1.

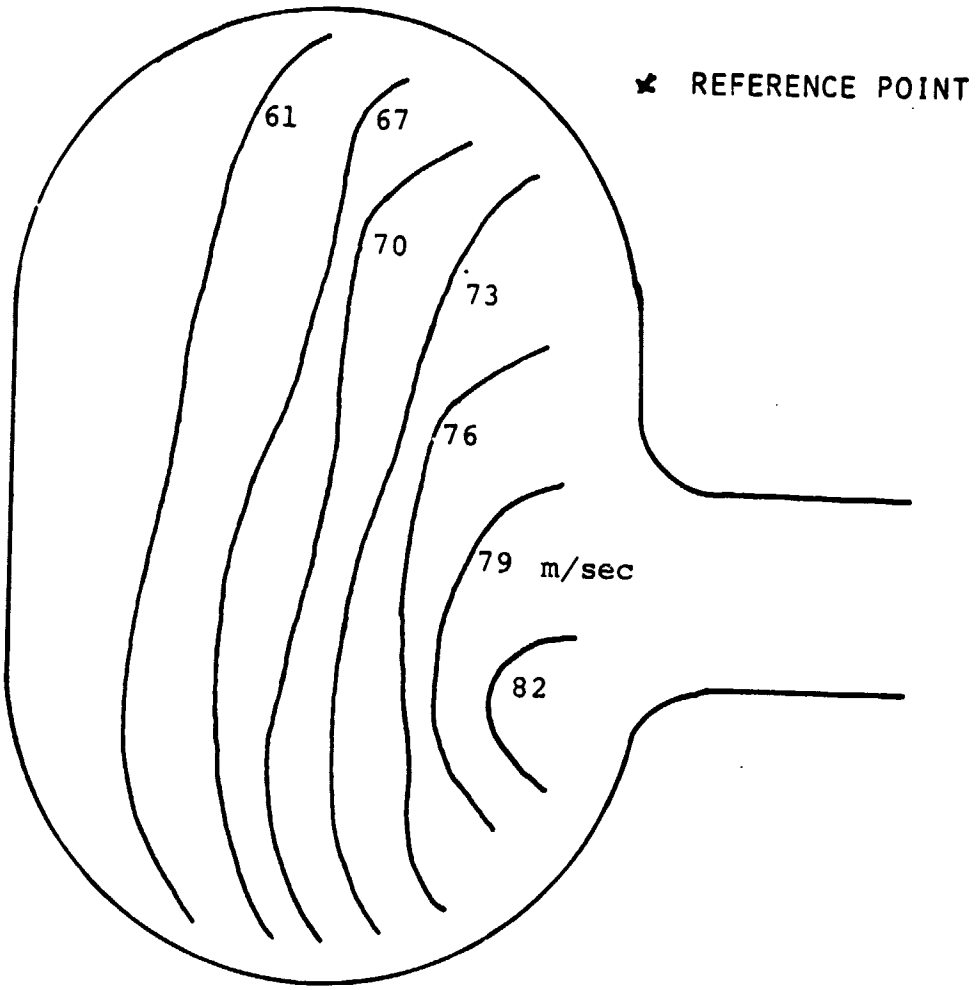

FIG. 8. THROUGH FLOW VELOCITIES, CROSS SECTION 2.

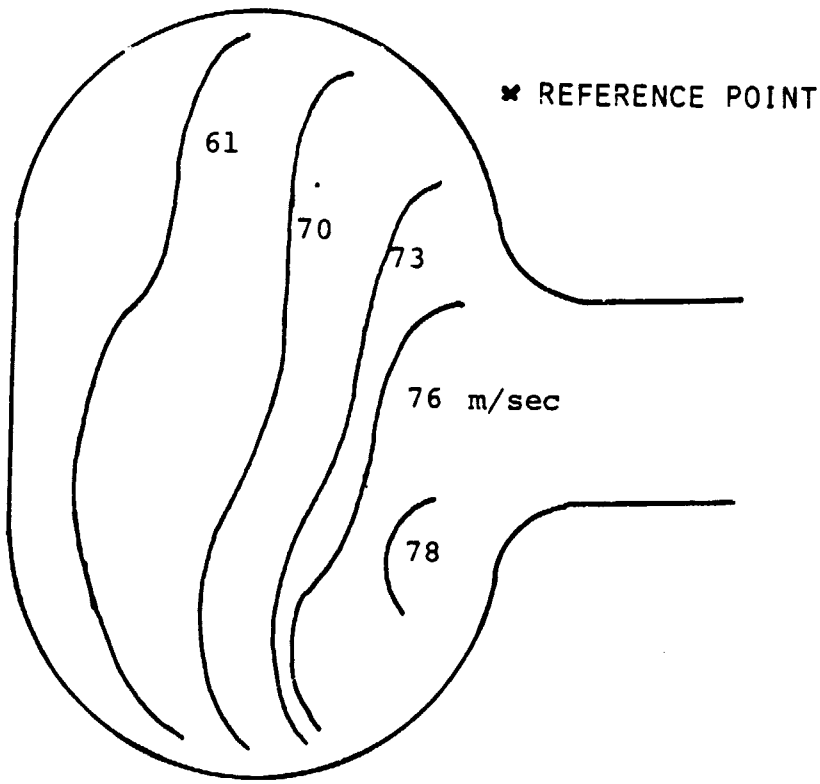

FIG. 9. THROUGH FLOW VELOCITIES, CROSS SECTION 3.

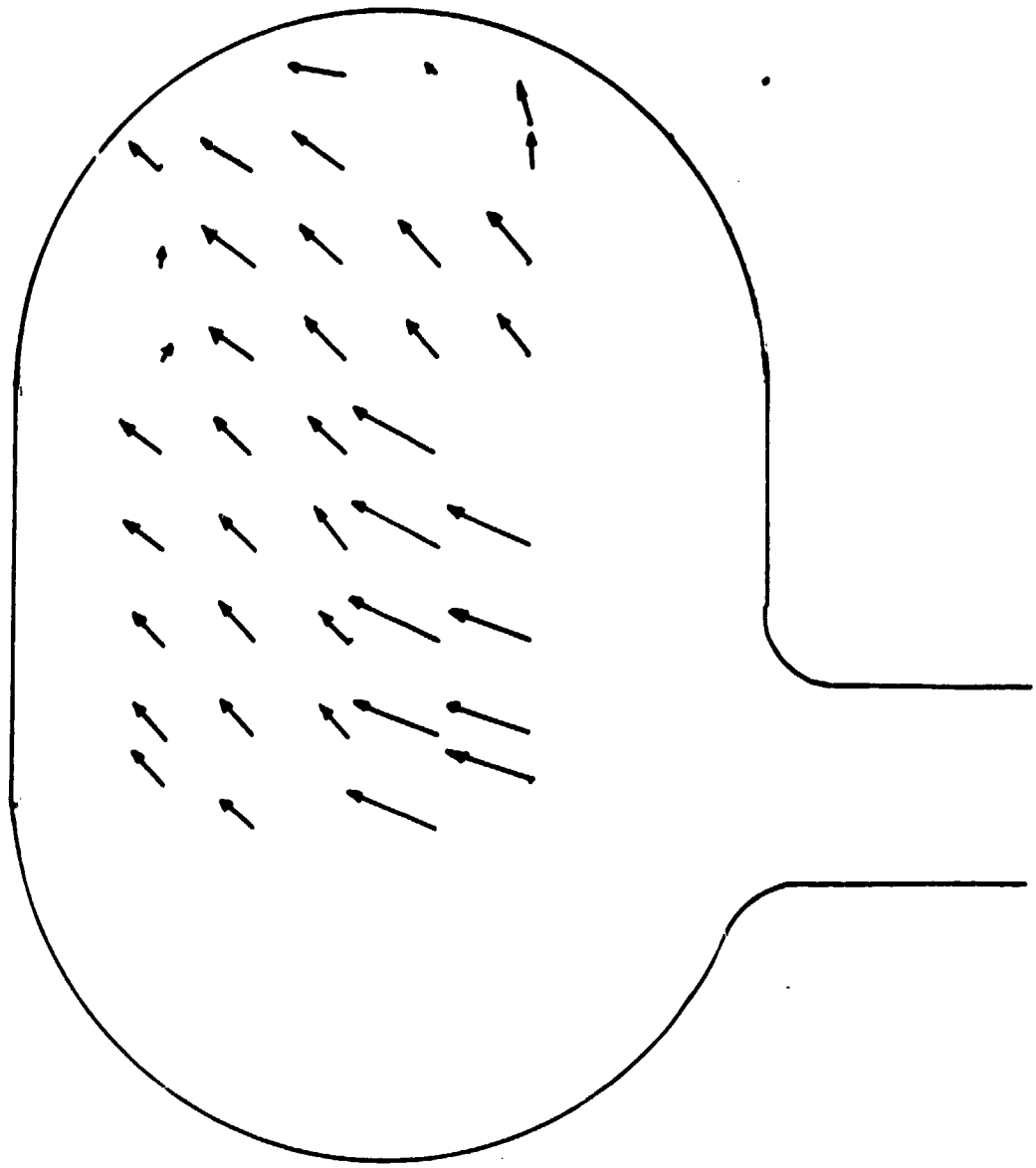

SCALE: 1 cm = 12 m/sec

FIG. 10. SECONDARY FLOW RESULTANT VECTORS, CROSS SECTION 1.

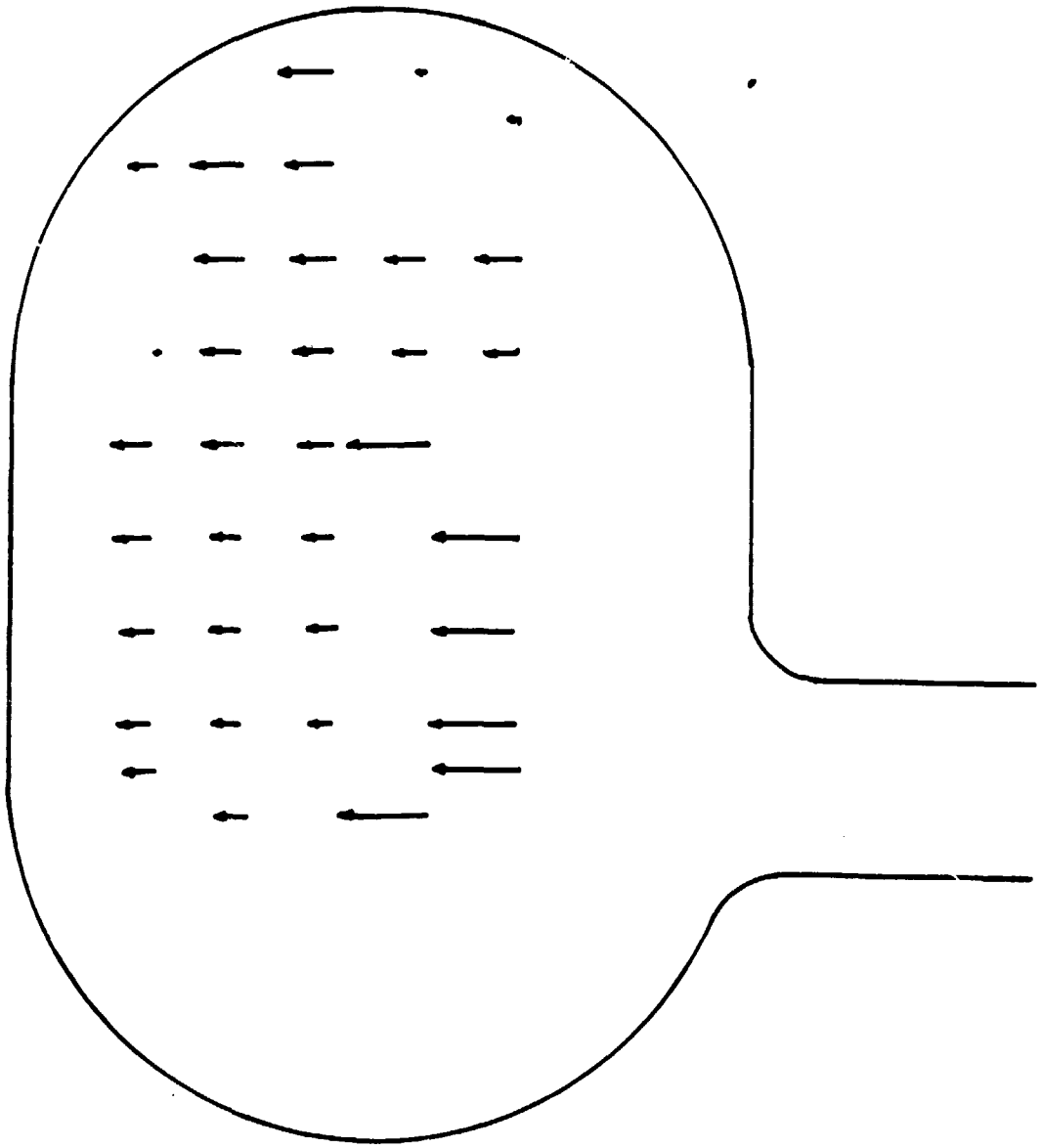

SCALE. 1 cm = 12 m/sec

FIG. 11. SECONDARY FLOW HORIZONTAL COMPONENTS, CROSS SECTION 1.

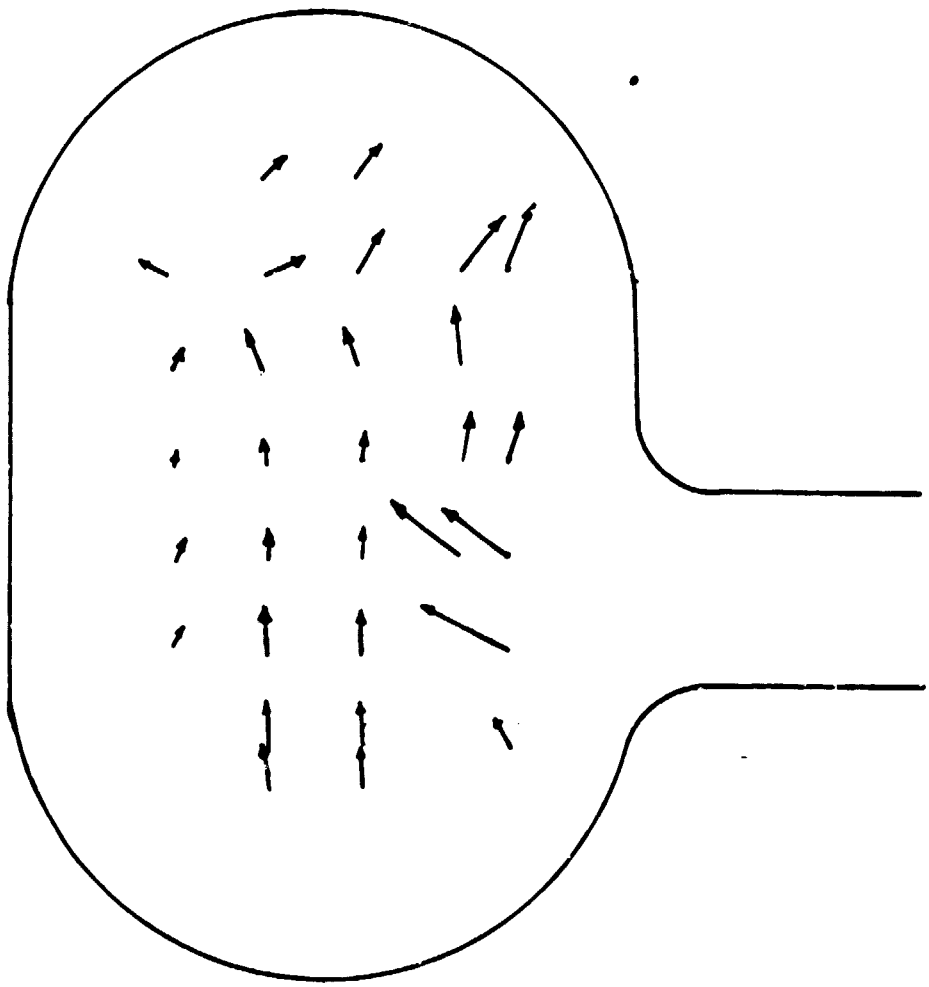

SCALE: 1 cm = 12 m/sec

FIG. 12. SECONDARY FLOW RESULTANT VECTORS, CROSS SECTION 2.

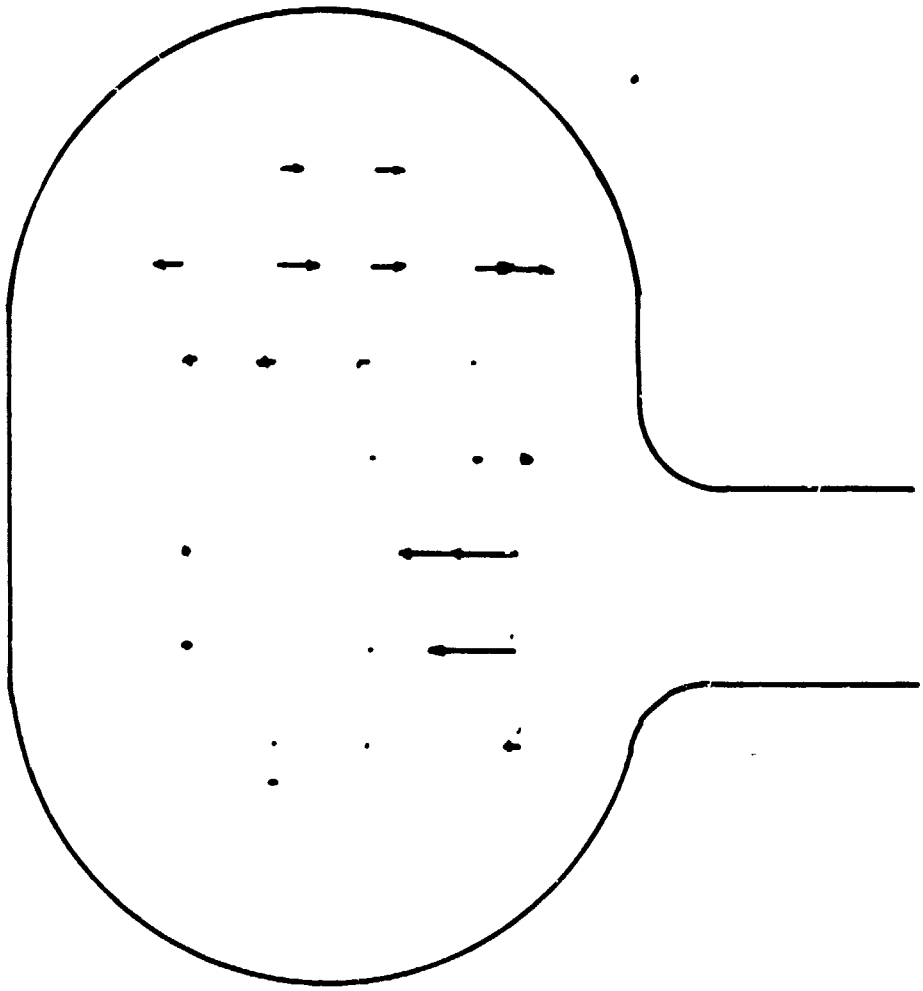

SCALE: 1 cm = 12 m/sec

FIG. 13. SECONDARY FLOW HORIZONTAL COMPONENTS, CROSS SECTION 2.

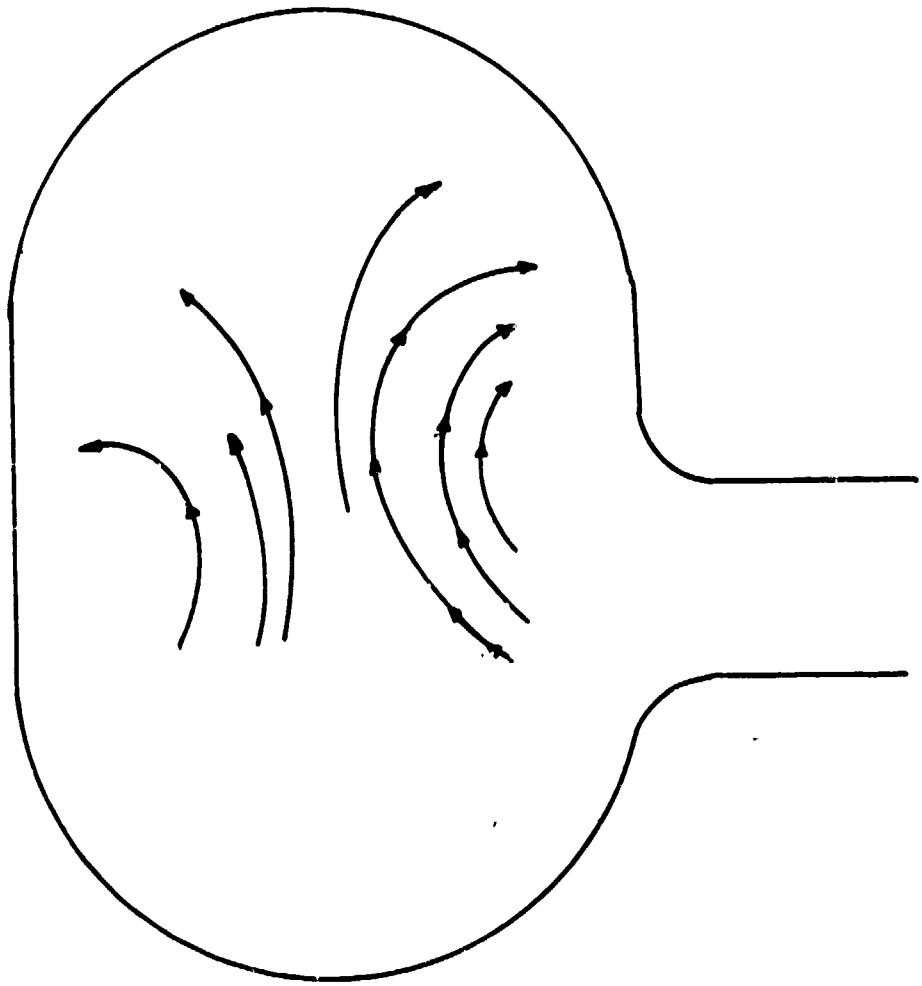

FIG. 14. SECONDARY FLOW DIRECTION, CROSS SECTION 2.

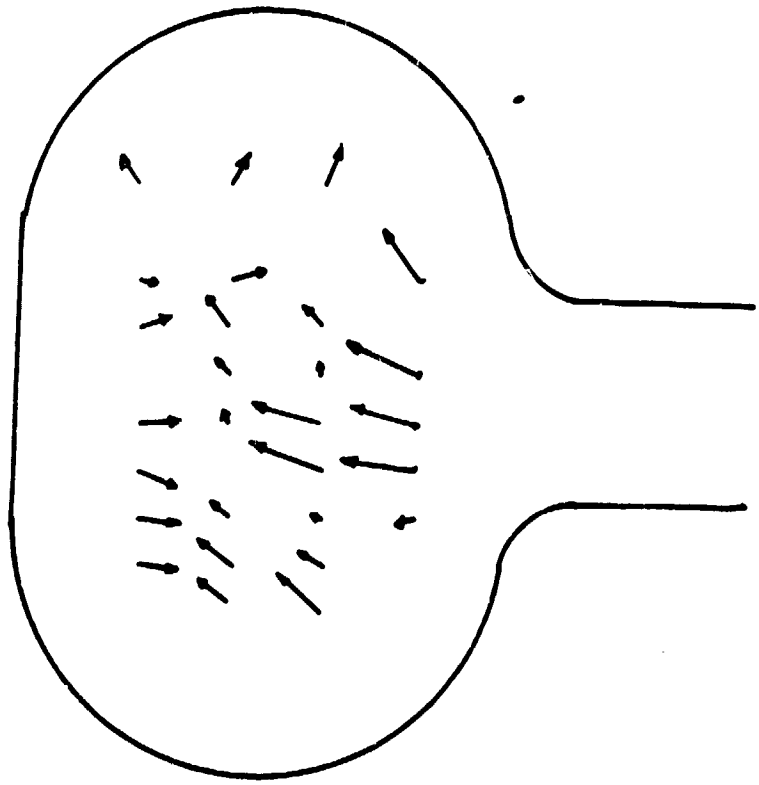

SCALE: 1 cm = 12 m/sec

FIG. 15. SECONDARY FLOW RESULTANT VECTORS, CROSS SECTION 3.

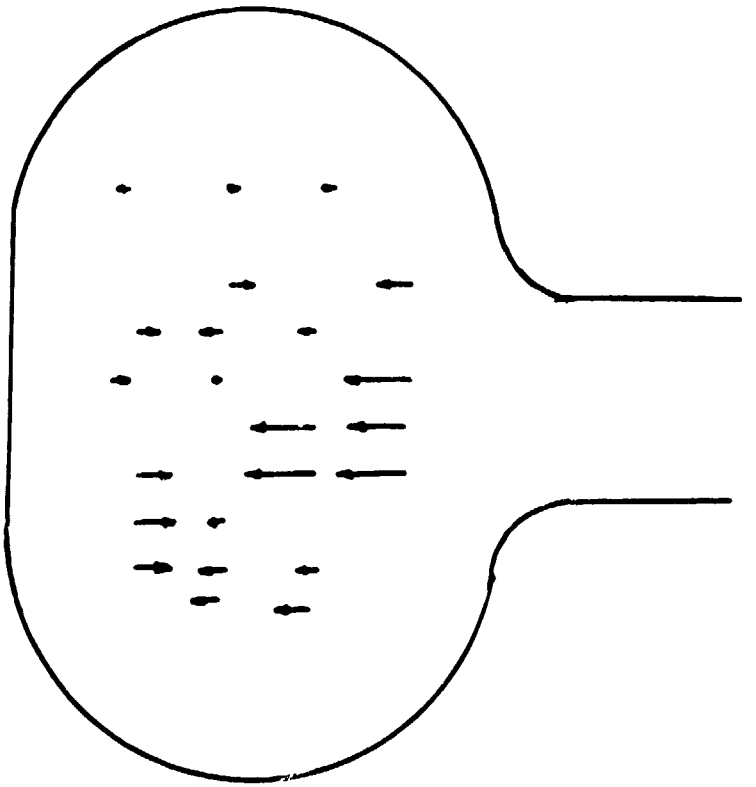

SCALE: 1 cm = 12 m/sec

FIG. 16. SECONDARY FLOW HORIZONTAL COMPONENTS, CROSS SECTION 3.

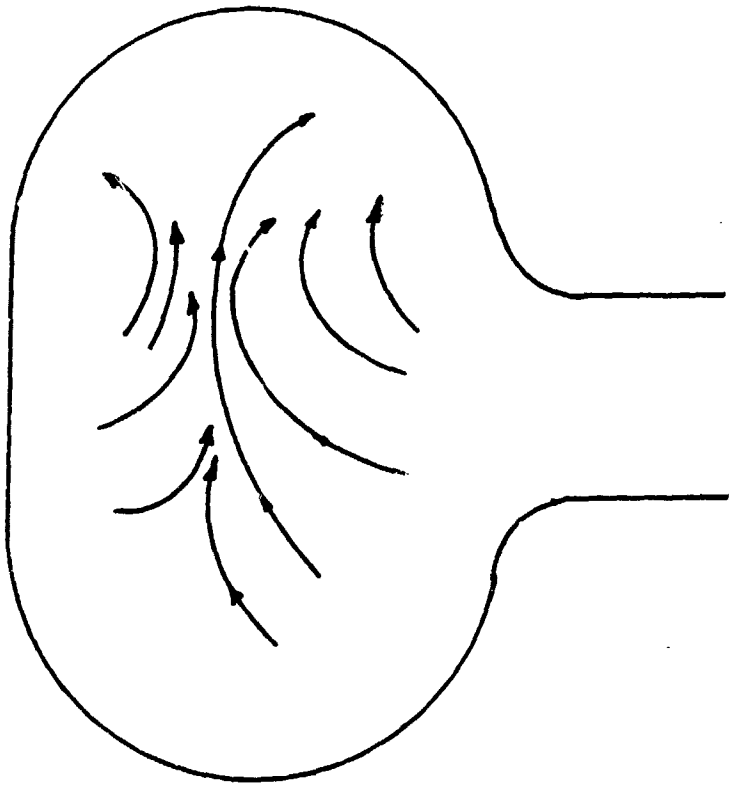

FIG. 17. SECONDARY FLOW DIRECTION, CROSS SECTION 3.

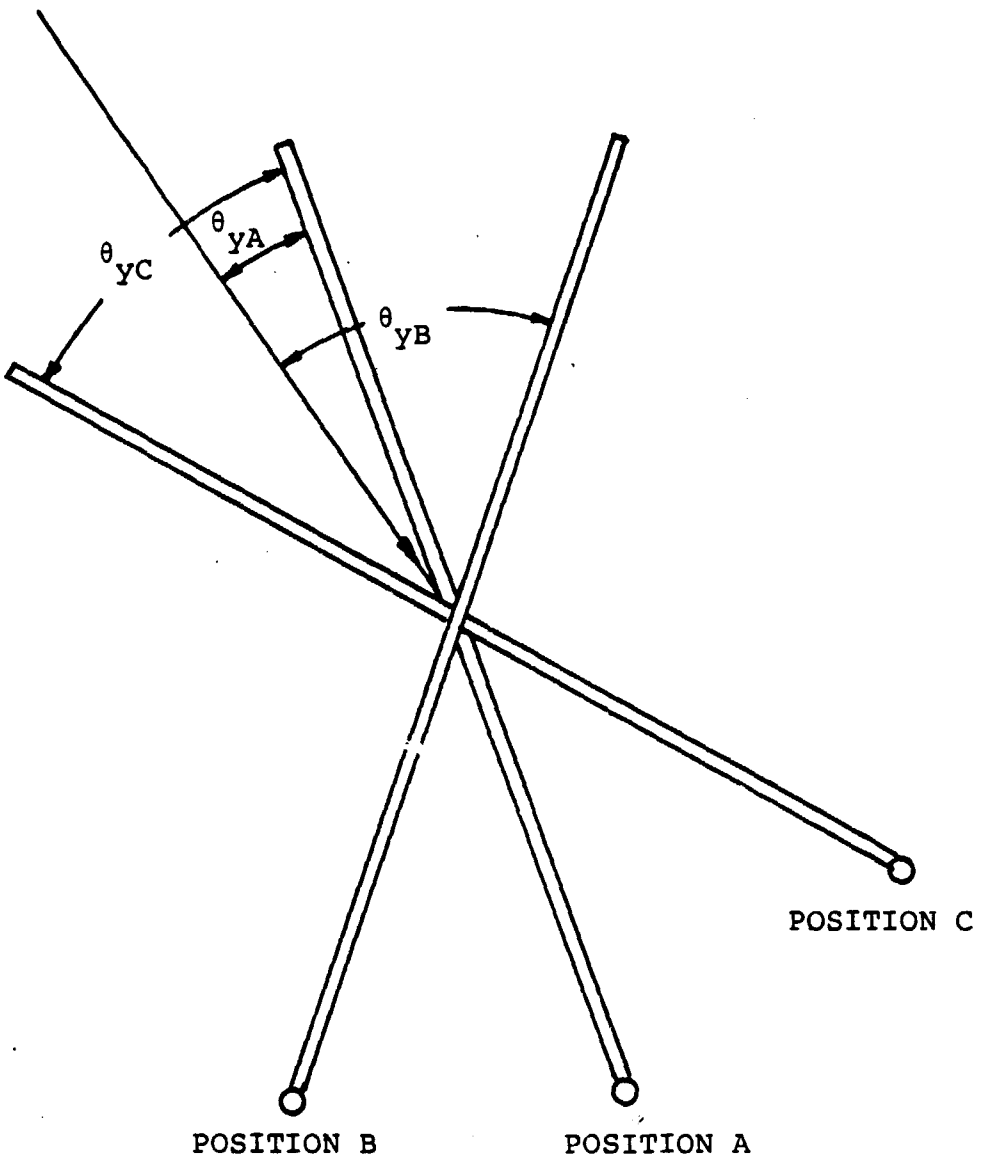

FIG. 18. MEASUREMENT TECHNIQUE.